JOURNAL OF GEOPHYSICAL RESEARCH, VOL. 99, NO. C5, PAGES 10,221–10,239, MAY 15, 1994

Observations of bottom currents and estimates of resuspended sediment transport at the New York Bight 12-mile dumpsite

J. P. Manning[1], L. Y. Oey,[2,3], D. Packer[4], J. Vitaliano[4], T. W. Finneran[4], K. W. You[3], and S. Fromm[4]

Abstract. To document storm events that may induce a redistribution of sediment in the vicinity of the New York Bight 12-mile sewage sludge dumpsite, current meter moorings were deployed in water depths from 20 m (near the mouth of New York Harbor) to 53 m (within the Hudson Shelf Valley) from July 1986 through June 1989. Ten usable instrument records ranging from one month to one year in duration were obtained; eight of them near-bottom records. Seasonal and geographic variability of wind-induced flow were examined. The wind is most efficient in driving the subtidal currents in the 2-10 day frequency band during winter when the water column is well mixed and when the eastward component of the wind often induces and sustains an up-valley (northward) bottom flow. Maximum efficiency occurs for wind from 300° (WNW) and at sites located within the Hudson Shelf Valley. A continental shelf bottom boundary layer model (Glenn and Grant, 1987) was used to estimate resuspended sediment transport. Model inputs include bottom currents (observed), orbital wave velocities (estimated), and sediment grain size (from the literature). Model output indicates that sediment resuspension at the current meter sites occurs approximately 5% of the time, primarily during winter months. The difference in along-valley flux between two moorings provides a rough estimate (6-month time series) of deposition and erosion. The net deposition (+.02 mm) was no greater than the deposition and erosion resulting from individual storms. A three-dimensional circulation model (You et al., 1991) is applied to increase the spatial resolution of the near-bottom current field (4 km grid) for a storm event in May of 1987. Given these velocities that vary in space and time, the redistribution of sediment was modeled for different surface wave conditions. Areas of deposition aligned with the Hudson Shelf Valley due to less wave-induced resuspension in deeper waters. Given all the uncertainties in the input variables (grain size, surface waves) and the simplistic assumptions made in modeling the deposition and erosion, it is still uncertain how much sludge is permanently removed from the area, but episodic redistribution of surficial sediment evidently occurs throughout the Inner New York Bight.

Introduction

For several decades, municipalities of New York and New Jersey dumped sewage sludge at a site located approximately 12 nautical miles east of Sandy Hook, New Jersey. In late 1987, after several years of litigation, the site was closed due to elevated levels of pollutants found in both the sediment and biota [*Environmental Processes Division,* 1987].

In July 1986, the National Marine Fisheries Service, an office of the National Oceanic and Atmospheric Administration (NOAA), initiated a 3-year multiagency observational program to monitor the response of habitat and biota to cessation of sewage sludge dumping. Biological, geological, and chemical samples were collected on a variety of space scales and timescales in order to assess environmental change [*Studholme et al.,* 1991].

One component of this multidisciplinary effort was the measurement of the near-bottom flow field to document storm events that may induce sediment erosion and transport. Current meters were moored near-bottom at several locations in the vicinity of the dumpsite from July 1986 to June 1989 (Figure 1). Our objectives are to (1) summarize these current meter records, (2) explain the current variability in terms of meteorologic forcing functions, (3) make order-of-magnitude estimates of resuspended sediment transport at bottom-current meter sites, and (4) examine factors governing the spatial distribution of deposition and erosion.

Much of the pre-1986 studies on the physical oceanography of the New York Bight occurred during the NOAA Marine Ecosystem Analysis (MESA) program in the mid-to-late 1970s. Using data from a set of current meter moorings, deployed for a period of 2 months in the fall of 1973 within the upper Hudson Shelf Valley, *Nelson et al.* [1978] were the

[1]National Marine Fisheries Service, National Oceanic and Atmospheric Administration, Woods Hole, Massachusetts.
[2]Atmospheric and Ocean Sciences, Princeton University, Princeton, New Jersey
[3]Department of Civil, Environmental, and Ocean Engineering Stevens Institute of Technology, Hoboken, New Jersey.
[4]National Marine Fisheries Service, National Oceanic and Atmospheric Administration, James J. Howard Laboratory, Highlands, New Jersey

Paper number 93JC03273
0148-0227/94/93JC-03273$05.00

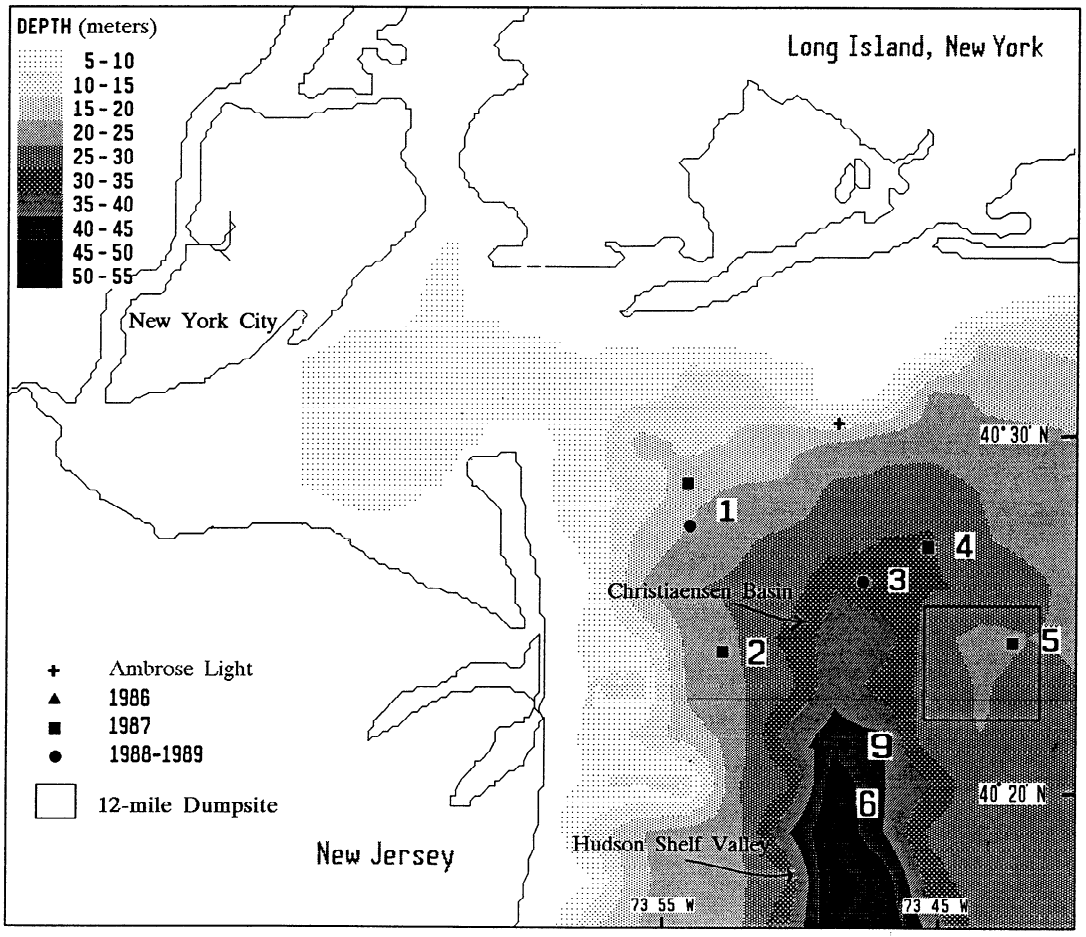

Figure 1. Current meter mooring locations relative to bathymetric contours and the 12-mile dumpsite.

first to present quantitative evidence of wind-induced along-valley flow. They were able to estimate an upvalley flow during the winter (October-April) and a downvalley flow during the remainder of the year by means of a simple model with local wind conditions as input. A more detailed model, including three-dimensionality and both wind and density driven dynamics, is presented by *Han et al.* [1980]. *Mayer et al.* [1982] summarized a more extensive (spring 1974 to spring 1977) set of current observations in order to present direct evidence of the wind-induced variability; eastward winds driving upvalley flow and vice-versa. They were able to show differences in the variability due to the cross-shelf location, depth, frequency, and degree of stratification.

The data reported in this paper, while adding to the existing MESA database, also provide time series of bottom currents throughout the year at a location which is closer to the 12-mile dumpsite and the shallow head of the Hudson Shelf Valley than previous measurements. MESA observations of wintertime currents were limited to sites further offshore (LT6 and LT7 in *Mayer et al.'s* [1982] paper). While most of the MESA studies reported bed load transport estimates [*Gadd et al.*, 1978; *Lavelle et al.*, 1978; *Vincent et al.*, 1981], this study focuses on an important mechanism of pollutant dispersion, the resuspension of fine surficial sediment. [*Clarke et al.*, 1982].

Methods

Data Collection

Moorings of vector-averaging current meters (VACM) were deployed near the head of the Hudson Shelf Valley in water depths ranging from 20 to 53 m. The objective was to document the degree of spatial variability that may be due to topographic and hydrographic conditions. The sites were chosen based on distance to the 12-mile dumpsite and the direction of local bathymetric gradients. Those moorings closer to the New Jersey shore, for example, were expected to show the effects of the Hudson River Plume.

Deployments for this study began with a single-pilot mooring in the summer of 1986 (Figure 1). This mooring had three instruments at depths of 14, 28, and 44 m below the sea surface. The bottom meter (44 m) failed because of an electronic problem. In May of 1987, seven moorings with bottom meters approximately 1 m off the bottom were deployed. Owing to both fish trawling and biofouling, portions of the 1987 records were lost, including two complete mooring records. Three additional moorings were deployed in May 1988, cleaned in November 1988, and successfully recovered in June 1989. Start and stop times for all usable raw data are listed in Tables 1a and 1b.

Table 1a. Raw Current Meter Statistics

Station	Water, Depth	Instru., Depth	North, Latitude	West, Longitude	Good Data Start	Good Data Stop	East Mean	East Std	East Min	East Max	North Mean	North Std	North Min	North Max	Speed Mean	Speed Std	Speed Max
1A	20	19	40°27.6	73°52.2	Jul.11,1987	Aug.18,1987	0.77	4.77	-15	25	-0.32	6.18	-20	36	6.13	4.90	37
B					Jun.27,1988	Oct.10,1988	-0.28	8.70	-25	26	-1.17	11.61	-24	32	13.38	5.73	38
C					Nov.16,1988	Jun.26,1989	-1.04	7.14	-28	28	1.17	10.50	-33	31	11.68	5.22	35
2	22	21	40°23.4	73°52.2	May 9,1987	Jul. 8,1987	-2.01	6.98	-21	18	-2.24	9.49	-27	21	10.98	5.21	31
3A	36	35	40°25.8	73°48.0	May 6,1988	Aug.31,1988	-1.02	5.36	-17	15	0.20	8.03	-18	23	8.89	3.88	24
B					Nov.16,1988	Jun.26,1989	-0.70	5.58	-27	16	5.08	9.81	-23	45	10.56	6.50	45
4	27	26	40°26.4	73°44.4	May 9,1987	Aug.16,1987	0.37	6.55	-16	18	-0.42	6.19	-20	17	8.30	3.56	20
5	26	25	40°24.0	73°44.4	May 9,1987	Jul.9,1987	-1.01	6.06	-15	20	-2.63	7.98	-26	17	9.46	4.32	27
6	53	52	40°19.2	73°47.4	May 9,1987	Aug.27,1987	-0.14	2.32	-10	9	1.08	9.25	-35	25	7.95	5.38	35
9A1	44	14	40°21.0	73°47.4	Jun.30,1986	Sep.28.,1986	1.63	10.40	-27	38	3.79	13.75	-40	43	15.40	8.77	46
9A2		28			Jun.30,1986	Oct.31,1986	0.03	5.77	-19	26	5.98	9.81	-20	64	10.08	7.99	65
B		41			Jun.26,1988	Jun. 6,1989	-0.72	3.90	-30	13	4.11	13.41	-50	54	12.22	7.94	55

East, eastward; North, northward; std., standard deviation. Units of depth are meters. Units of mean, std, min, and max are cm/s.

Table 1b. Wind Statistics

Station	Water, Depth	Instru., Height	North, Latitude	West, Longitude	Good Data Start	Good Data Stop	East Mean	East Std	East Min	East Max	North Mean	North Std	North Min	North Max	Speed Mean	Speed Std	Speed Max
Ambr	25	49	40°30.0	73°48.0	May 5,1986	Oct.30,1986	1.56	4.77	-16	13	0.22	4.98	-17	14	6.29	3.23	18
Light					Jan. 1,1987	Dec.31,1987	0.84	5.55	-19	17	-1.10	5.46	-21	20	7.00	3.70	23
Towr					Jan. 1,1988	Dec.31,1988	2.45	4.93	-21	17	-0.57	5.82	-20	18	7.15	3.66	22
					Jan. 1,1989	Jun. 6,1989	0.96	5.62	-22	15	-0.52	5.47	-20	18	6.98	3.73	22
					Jan. 1,1990	Jun.30,1990	2.15	5.83	-18	16	-0.16	6.15	-20	18	7.81	3.94	22

East, eastward; North, northward; std., standard deviation. Units of depth and height are meters. Units of mean, std, min, and max are m/s.

Environmental data, collected at offshore NOAA tower and buoy stations, were obtained from the National Climatic Data Center (NCDC) and the National Oceanographic Data Center (NODC). Hourly average wind velocities were available for the entire study period from Ambrose Light Tower (Figure 1), located a few miles north of the study area. Surface wave information was also available for the entire study period from either Delaware (buoy 44012) or Nantucket (buoy 44008). Surface wave information from Ambrose Light Tower and the Nantucket buoy, collected concurrently for the first 6 months of 1990, was obtained as well.

Sediment samples were taken at three "replicate" sites (squares in Figure 2) on a monthly basis during the study period in order to monitor levels of bacteria, trace metals, and grain size [*O'Reilly et al.*, 1994; *Zdanowicz et al.*, 1994; *Packer et al.*, 1994]. While most of the analysis reported in this paper used the grain size information (stars in Figure 2) reported earlier by *Hathaway* [1971], new grain size information became available (triangle in Figure 2) from *Packer et al.'s* [1994] study.

Sediment samples were also taken at 22 "broadscale" sites (circles in Figure 2) bimonthly during the study period. Characteristics such as sediment type, porosity, and percent fines (fraction of particles <63 μm) were determined for each sample. Methods used in sediment sampling are reported by *Packer et al.* [1994].

Data Processing and Analysis Methods

The current, wind, wave, and sediment data were processed as follows:

Observed currents. Hourly averaged current meter data were used for tidal analysis and sediment transport calculations. A 33-hour low-pass filter [*Flagg*, 1977] was used in the case of wind current analysis, however, to remove the diurnal and semidiurnal tides. Standard spectral analysis techniques were applied to the current meter and wind data to compute the coherence and phase between sites, including both current-current and wind-current relationships.

Modeled currents. A three-dimensional circulation model, as described by *You* [1992], includes the response of current and density to wind, tide, river, atmospheric heating and cooling, and open ocean forcing. At each 4 km grid point the velocity was computed in 10 separate layers of the water column, which varied according to water column depth. The deepest (near-bottom) layer is used in this study.

Winds. Hourly averaged wind speed recorded at 49 m above sea level at Ambrose Light Tower was first filtered to remove spurious data by replacing any values greater than 2 standard deviations from a 10-hour running mean with that same mean. The filtered values were then converted to wind stress at the air-sea interface according to the method of *Large and Pond* [1981]. Computed wind stress (dyne per square centimeter) values were then used to compute wind-

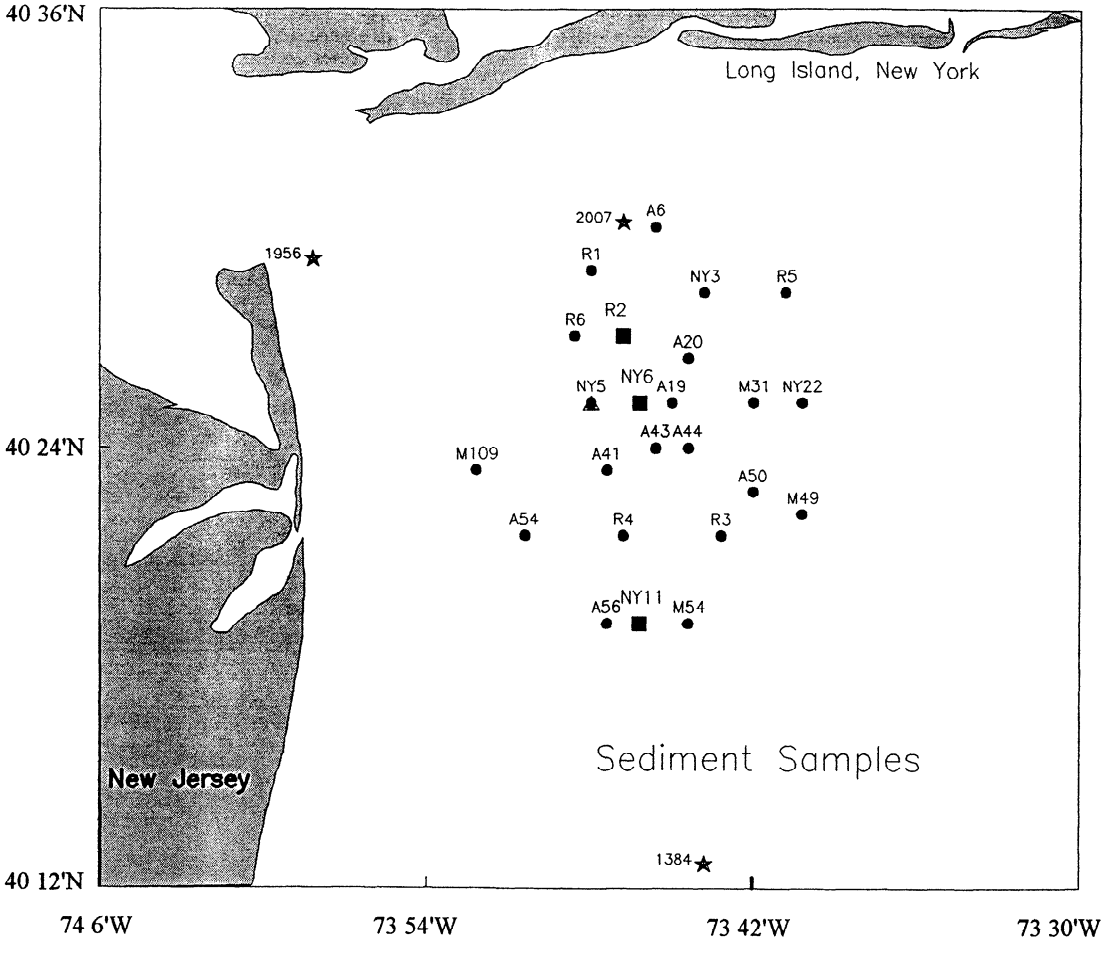

Figure 2. Location of "broadscale" stations (circle), "replicate" stations (squares), station NY5 (triangle), and *Hathaway* [1971] stations (stars). Grab samples were taken for sediment analysis at all of these sites.

current relationships. In order to test the efficiency of wind in driving the subtidal bottom flow (V), a transfer function (H) was calculated as a linear response to the Ambrose Light Tower wind stress (W)

$$V(f) = H(f)W(f)$$

where f represents frequency. H(f) is nonzero only at frequencies for which the input (W) and the output (V) are significantly coherent.

Waves. Linear wave theory was used to estimate near-bottom wave characteristics. The entire wave spectrum for each hourly observation, supplied by NODC, was used to determine the dominant wave heights and frequencies. The resultant root mean square (rms) orbital wave velocity and excursion amplitude were calculated for each hourly observation.

Since wave information was not recorded at Ambrose Light Tower during the deployment period, remote observations were used. First, a correction factor (gain) and a lead (phase) time were calculated on the basis of 6 months of simultaneous measurements at the Nantucket buoy and Ambrose Light Tower in the spring of 1990. Gain factors of .45 and .59 for rms orbital velocity and excursion amplitude, respectively, were applied with a 9-hour lead time to generate a wave series for Ambrose Light Tower. These figures were obtained for the 2-10 day band (coherence, .64). The Delaware buoy data was used directly.

Sediments. Sediment grain size distributions reported by *Hathaway* [1971] were proportioned into four sediment phi classes for each site (see Table 2). These data were used as input to the sediment transport model. As more sediment data became available [*Packer et al.*, 1994], tests were conducted on the sensitivity of sediment transport estimates to grain size distributions. The sediment data collected during this study period on the broadscale surveys were used to describe the general characteristics of the sediment. Distribution maps were generated to provide a rough picture of the spatial variability in percent fines (top 5 cm) and sediment type (top 1 cm).

Sediment resuspension and transport estimates. In order to estimate the temporal variability of resuspended sediment transport at individual sites, a bottom boundary layer model [*Grant and Madsen*, 1979; *Glenn and Grant*, 1987] was applied to the data from the second and third current meter deployments. Inputs to the model include (1) estimated amplitudes (1.41*rms) of bottom orbital wave velocity, (2) estimated amplitudes of bottom wave excursion, (3) observed currents at 1 m above the bottom, and (4) sediment grain size distributions. The model accounts for the nonlinear wave/current interaction, sediment-induced stratification, variable fall velocities for different grain sizes, changes in bottom friction due to the formation of ripples and moveable bedforms, and the associated modifications of velocity in the near-bottom layer. A detailed description of the model is given in *Glenn and Grant* [1983] and sensitivity studies are reported in *Goud* [1987]. Outputs of the model include estimates of sediment concentrations above the bottom and, given the estimated velocity profile, the associated sediment transport in those same layers.

Deposition/erosion estimates. To examine the temporal variability of deposition and erosion events, the difference in

Table 2. Sediment Grain Size Data

				Phi Sizes (%)															
				Hathaway [1971]							Packer et al. [1994]								
Date	Sta#	Latitude	Longitude	0	1.5	2.0	2.5	3.0	3.5	4.0	<1	2	3	4	6	8	>8
October 15, 1963	1384	40°14.5	73°43.8	0	0	0	16	22	52	7							
July 26, 1964	1956	40°29.1	73°58.2	24	31	0	0	35	0	11							
August 7, 1964	2007	40°30.1	73°45.9	0	0	38	29	17	16	0							
March 15, 1989	NY5	40°25.5	73°48.4								3	1	9	61	11	3	10
September 15, 1989	NY5	40°25.5	73°48.4								8	54	32	2	0	0	4

The depth of sediment measured was approximately 20 cm and 5 cm, respectively, for the two studies.

along-valley sediment transport at moorings 3 and 9 for the 6-month period of January-June 1989 was calculated. Observed current velocities and the corrected Nantucket wave data were input to the sediment transport model. Since we are only interested in along-valley gradients in this highly idealized model, the cross-valley gradients are set at zero. What comes into one side of the box is not the same as what exists the other side. The difference gets deposited on (or eroded from) the bottom. The single box extends from mooring 3 (36 m) to mooring 9 (44 m) over a 8.5 km along-valley distance. Since this estimation of deposition and erosion is more of an exercise than a realistic simulation, the results are presented in the discussion section.

To examine the processes that influence the spatial distribution of deposition and erosion, a three-dimensional circulation model was employed. Given a subset of the near-bottom velocities covering the area of the 12-mile dumpsite, estimates of sediment transport were made for a typical storm (late May 1987). Given the estimates of sediment transport at 64 grid points, mean sediment flux through each side of each 4 km square was calculated. Estimates of deposition/erosion were made within each square. Several runs were made under different cases of surface wave conditions. As in the temporal variability case, the results are presented in the form of discussion.

Results

Observed Currents

Basic current statistics for the entire deployment period are listed in Tables 1a and 1b. The mean, standard deviation, and range at each site are listed for both the eastward and northward unfiltered raw velocities, as well as the vector speed. The maximum flow is shown to be an order-of-magnitude greater than the mean and, sometimes, in the opposite direction of the mean. At mooring 6, for example, the mean flow is to the north at about 1 cm/s, but the maximum flow was recorded to the south at 36 cm/s. The standard deviations are also much greater than the means.

Time series of the low-pass filtered bottom currents for all deployment periods are plotted in Figure 3 along with the eastward wind stress. The two upper water column records (9A1 at 14 m and 9A2 at 28 m) from the 1986 deployment show that as the season progressed into fall, the currents increased and were, in general, directed towards the north. For the summer of 1987 (1A, 2, 4, 5, and 6), the channelized flow of the deeper Hudson Shelf Valley site is depicted by the north/south (along-valley) orientation of the lowermost stick plot (6). The large event on May 21, 1987, indicating strong downvalley flow, is apparent at sites 2, 4, and 5, however, the flow was weaker and the current direction was more variable. For the full year deployment of June 1988 through June 1989 (1B, 1C, 3A, 3B, and 9B), the largest events are directed upvalley in the winter and appear to persist for several days. Examples of this persistent upvalley flow can be seen at all three moorings around December 1, 1988, and February 8, 1989.

The distribution of currents with respect to direction, speed, and frequency are presented in Figures 4a, 4b, and 4c, respectively. Polar bar charts in Figure 4a indicate (1) persistence of the currents along-valley orientation, (2) persistence of the winds eastward orientation, and (3) lack of "extreme" (>20 cm/s) during the summer season. While the peak in the distribution of current lies in the 5-10 cm/s range (Figure 4b), the less frequent extreme currents are the focus of this investigation. The distribution of current variability versus frequency is presented in Figure 4c in terms of spectral density. While the spectrum peaks as expected for the semidiurnal tide and its harmonic, most of the energy is associated with the lower-frequency (wind driven) cycles.

Progressive vector diagrams for all three current meter deployments are given in Figure 5a. The two good records from 1986 indicate a northeastward and northward flow for the surface (14 m) and middepth (28 m) layers, respectively, with most of the distance covered during the last two months, September and October. Records from the summer of 1987 demonstrate the spatial variability that may be observed over a period of one to three summer months, and the relatively stagnant conditions of that season. In the final deployment shown in the rightmost panel, mooring records 1C, 3B, and 9B depict strong northward flow during the winter months (December-February). If a water parcel traveled at the speed measured at site 9B, for example, it would cover approximately 500 km in 3 months time. Apparently, there is a region of strong divergence north of the study area.

The wind stress variability, represented by cross-hatched ellipses in Figure 5b, is multidirectional (low ellipticity) unlike the current variability which has larger north/south component. Low-frequency energy is equal to or larger than the tidal energy in the case of the middepth records (summer 1986) and at those sites that include wintertime measurements (winter 1988-spring 1989).

Table 3 lists the coherence and phase of current meter deployments 1C, 3B and 9B for the 2-10 day band. The values in the upper right refer to the north/south flow and those in the lower left refer to the cross-valley east/west flow. While the along-valley flow is fairly coherent among the three mooring locations, the cross-valley flow is far less coherent. Hence while the cross-valley flow is small compared to the along-valley flow, it is evidently more sensitive to the different bathymetric gradients or the exact orientation of the valley. The phases computed for each pair (relative to 2-10 day band) are given in hours where, for example, the value "9.5 (5.8)" indicates that the east/west flow at mooring 9B leads that at mooring 1C by 9.5 hr ± 5.8 hr with 95% confidence. Since this is the largest lag (minus)/lead (plus) between moorings, it appears that the mooring sites respond rapidly within this frequency bank.

Modeled Currents

The three-dimensional circulation model, while developed for purposes other than estimation of sediment transport, provides a relatively high-resolution representation of the near-bottom velocities throughout the inner New York Bight. A time series of modeled versus observed currents for the grid point closest to mooring 6 is depicted in Figure 6. Modeled daily average flow at all the grid points during May 20, 1987, is comparable to the observed flow (Figure 7). While a direct comparison is difficult to make since there are slight differences in the horizontal (1-2 miles) and vertical (2 m) positions of the model site and the observed site, the agreement in terms of direction of flow and response to a large wind events is enough for this preliminary investigation.

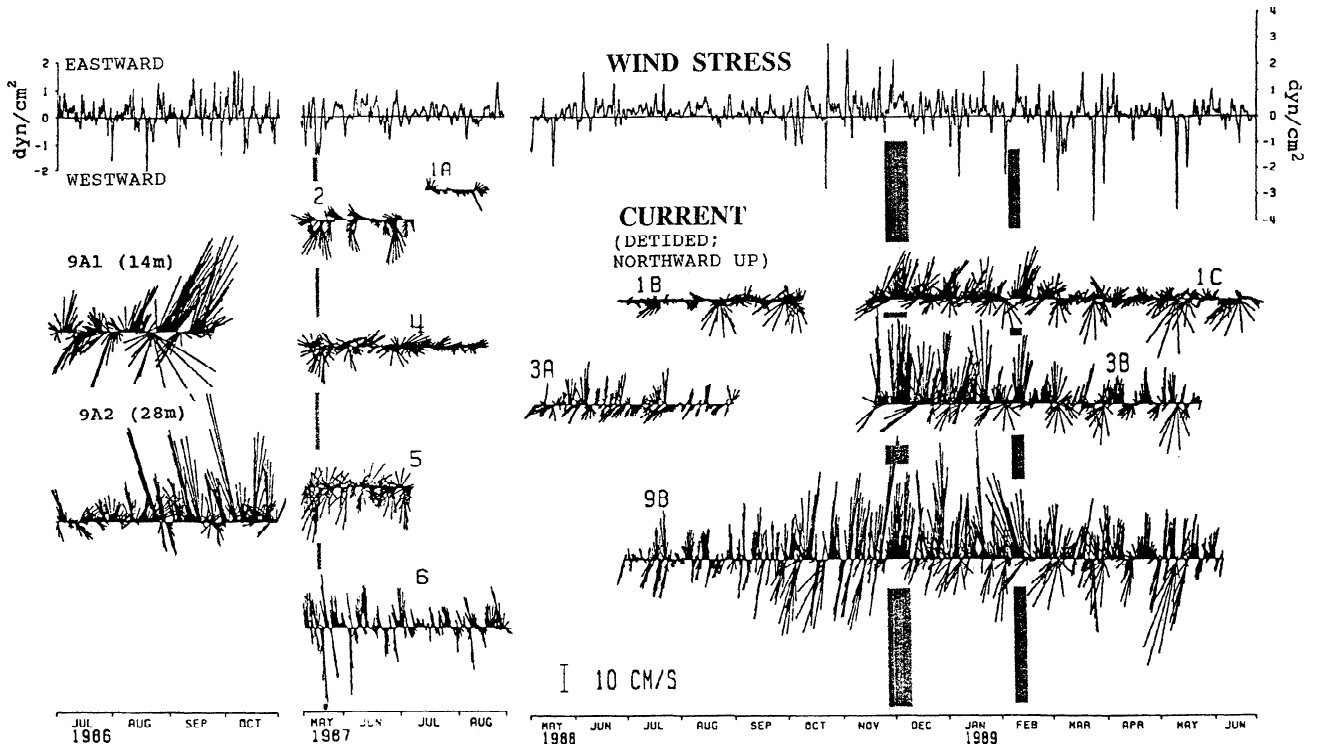

Figure 3. Low-passed current vectors for all current meter deployments (stick plots) and the eastward/-westward wind stress from Ambrose Light Tower (top panel) all subsampled 4 times daily. All current measurements are near bottom except for those in the 1986 deployment. Stippled bars indicate events discussed in the text.

A complete model verification is given in *You* [1992]. The model has been run for the entire year of 1987 with several simulations per day. Plans are underway to continue the program to hindcast 1988 and 1989 as well and to increase the spatial resolution to 2 km. Increasing the horizontal resolution may significantly improve the model in the region of the Hudson Shelf Valley. As depicted in Figure 6, the present version of the model (4 km resolution) underestimates the along-valley (channelized) flow.

Sediment Transport

Estimates of resuspended sediment transport are given in Table 4. Units are vertically integrated sediment concentration times velocity

$$\int (C(z)\ V(z))\ dz$$

with both concentration and velocity varying over 25 layers within 1 m of the bottom. In cgs units this may be written as

$$\int (\text{cm}^3 \text{ of sediment/cm}^3 \text{ of water})\ (\text{cm/sec})\ dz$$

which reduces to square centimeters per second.

The results indicate a very sporadic occurrence of transport that occurs primarily during the winter months and most often toward the north. As discussed below however, the "mean" values are the result of only a few events that are orders of magnitude larger than other events and may not be representative of the long-term character of the entire region.

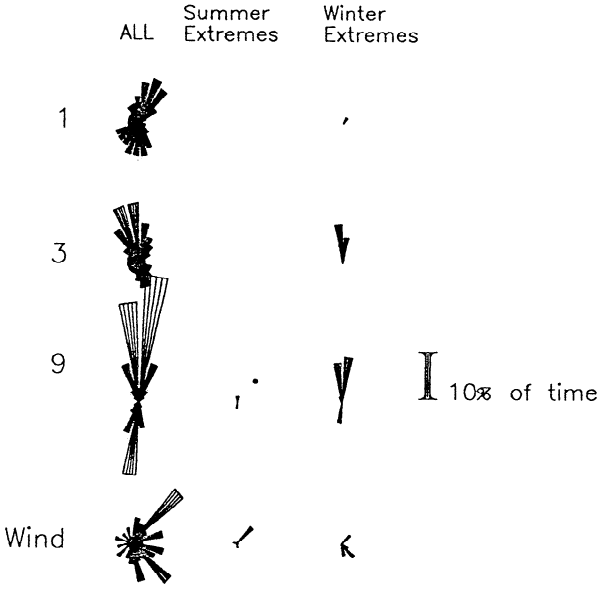

Figure 4a. Distribution of unfiltered current with respect to direction at sites 1, 3, and 9, and Ambrose Light Tower (wind) for the period of June 1988 through June 1989 including all, extreme summer, and extreme winter observations in the left, middle, and right column, respectively. "Extreme" represents observations of >20 cm/sec current and >20 knot wind. Length of arrow, as shown in legend on the right, refers to % time. Extreme current is usually towards the north and occurs in winter.

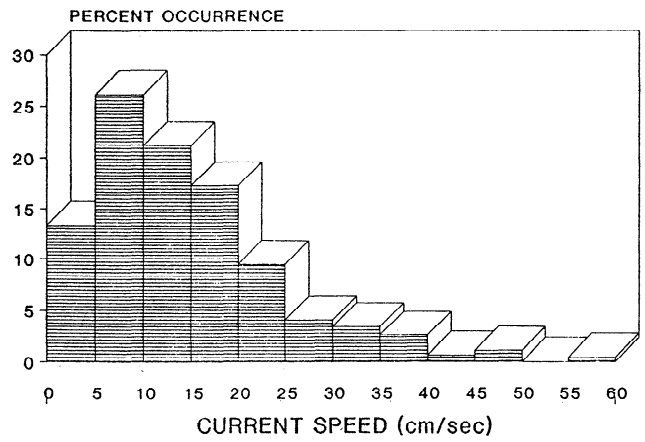

Figure 4b. Distribution of unfiltered current with respect to speed at site 9 for the full year June 1988 through June 1989.

Nevertheless, both the episodic (event-driven) and seasonal nature of the estimated transport can be examined more closely with stick plots presented in Figure 8. The top panel is the orbital wave velocity estimated off Delaware and Nantucket for the second and third deployments, respectively. In order to depict more than a few large events, it was necessary to log-transform the sediment transport data. (Note that the values less than 10^{-7} cm^2/s are not plotted.) During the second deployment there was a single event in late May 1987, mentioned above, where the orbital wave velocities exceeded 20 cm/s simultaneously with a strong downwelling event (Figure 3) mentioned earlier. The third deployment documents another relatively quiet summer period followed by several upvalley (northward) transport events that occurred in the winter of 1988-1989. If the arithmetic values for sediment transport are plotted in this way (rather than in order of magnitude), the smaller, multidirectional events, such as those observed in October 1988, would appear insignificant compared to the upvalley winter events. Whether they are indeed "insignificant" will be discussed.

Discussion

Wind-Current Relationship

Table 5 includes the coherence, gain, and phase between the eastward wind stress and the northward flow at all sites. Values are listed for low-frequency (<.5 cycle/d) currents only because higher-frequency relationships were not significant. Coherence estimates indicate that nearly half of the low-frequency current variability is explained by the wind. Gain factors range from approximately 4.0 at mooring 1 to 13.0 at mooring 6 indicating that the wind forcing is several times more efficient at the deeper, Hudson Shelf Valley site. Phase factors range from 0° to 85°, indicating that there is a quick set up time, usually less than 1 day, between the wind and current velocity in the 2-10 day band.

In order to determine the wind direction that was most efficient in driving the along-valley flow, the coherence and phase between the flow and the component of the wind in 15° intervals around the compass were calculated. The result indicates (Figure 9) that the winds from the WNW were most effective in driving the current.

In order to determine whether the winds recorded during the study period were representative of the historical mean wind, the winds recorded at Ambrose Light Tower (1987-1989) were compared to those recorded at New York City (NYC) and J.F.Kennedy (JFK) Airport (1948-1965; National Climatic Data Center, personal communication, 1993). Since there is obviously differences in the magnitude of the winds measure at the three different recording stations (NYC, JFK,

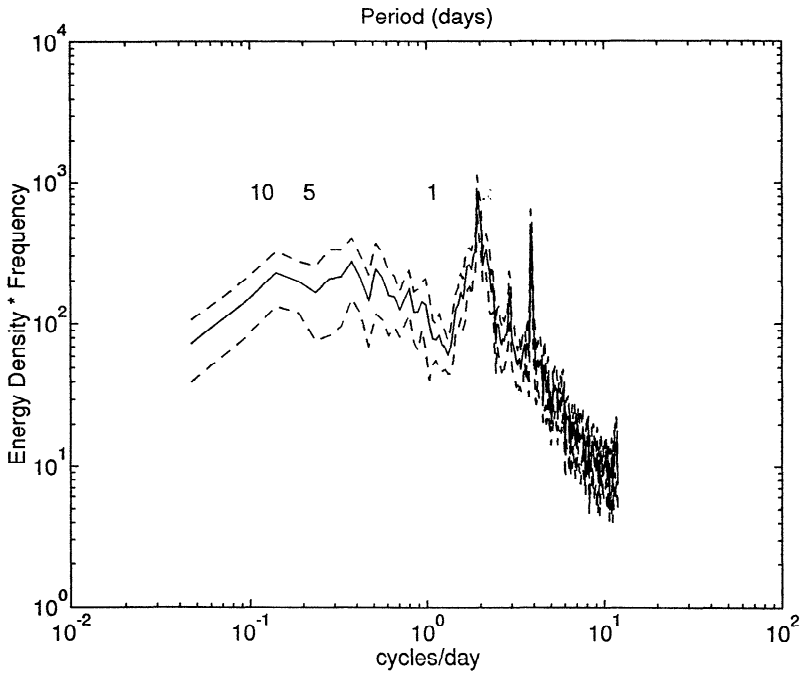

Figure 4c. Distribution of unfiltered current with respect to frequency at site 9 for the full year June 1988 through June 1989. Power spectral density units are $(cm/sec)^2/(cycles\ per\ day)$. The dashed lines represent the 95% confidence limits.

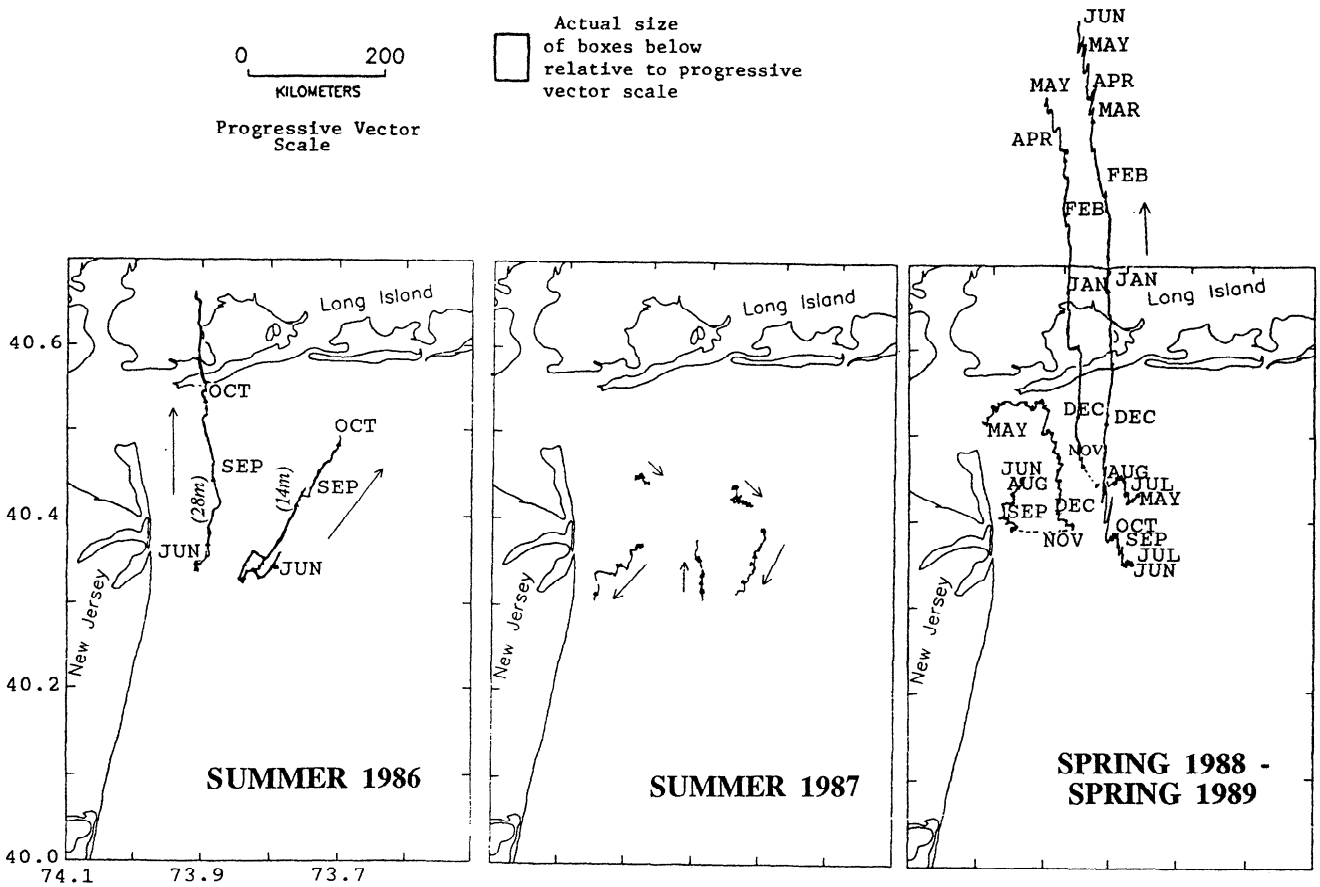

Figure 5a. Progressive vector diagrams for all three deployment periods. Arrows indicate general direction of flow. To prevent clutter, the starting positions for instrument records 9A2, 1B, and 3B are slightly offset from the actual mooring sites.

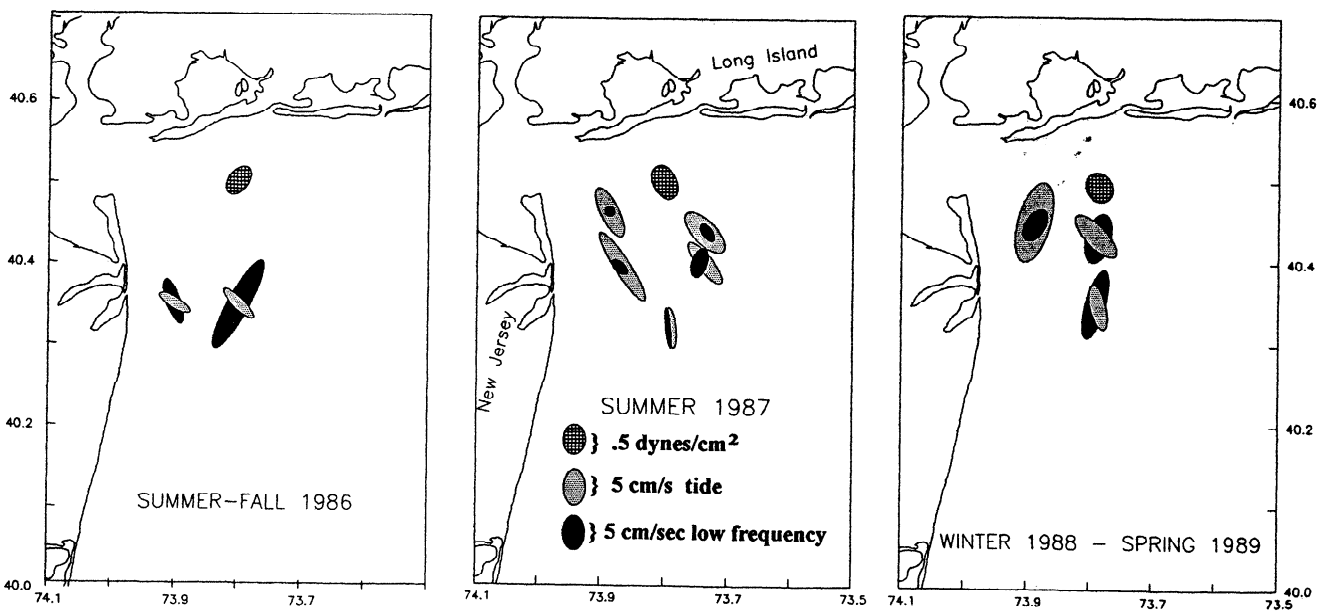

Figure 5b. Current ellipses for time periods similar to those shown in figure 5a (excludes summer/fall of last deployment). Cross-hatched ellipses represent standard deviations of wind stress. Stippled and solid ellipses represent standard deviation of the M2 tide and low frequency flow, respectively.

Table 3. Coherence and Phase Between Current Meter Mooring Sites for 2-10 Day Band

Station	Station 1C	Station 3B	Station 9B
Station 1C			
Coherence		.83 (.33)	.83 (.33)
Phase		-5.5 (2.8)	-1.8 (2.5)
Station 3B			
Coherence	.54 (.33)		.94 (.33)
Phase	-1.8 (6.3)		3.0 (1.3)
Station 9B			
Coherence	.57 (.33)	.63 (.33)	
Phase	9.5 (5.8)	8.5 (5.)	

Values on the upper right refer to along-valley (N/S) flow. Values on the lower left refer to cross-valley (E/W flow. Values within parentheses refer to 95% confidence intermal. Units of phase are in hours.

and Ambrose), a correction factor is needed. Averaged over the entire data set, the wind at the Ambrose Light Tower was 10% stronger than the winds measure on the land-based stations (NYC and JFK). If we consider "strong" winds those greater than 11 knots at the landbased stations, then "strong" winds at Ambrose Light Tower, given the 10% factor, are defined as those greater than 12.2 knots. Given these definitions, "strong" winds occurred approximately 11% more frequently (52% versus 41% of the time) during the study period (Figure 10). While the winds during the study period included anomalously strong southwesterlies, the majority of the time, as in the historical case, strong winds came from the upwelling-favorable northwest quadrant.

Wave-Current Induced Resuspended Sediment Transport

Determining the dominant forces governing bottom flow, however, is only the first step in estimation of sediment transport in and around the 12-mile dumpsite. The estimated orbital wave velocities, an important resuspension mechanism, along with low-frequency bottom current records at all sites (except for the summer of 1986 when near-bottom current was unavailable) were input to an empirical bottom boundary layer model.

Before interpreting the results listed in Table 4 and depicted in Figure 8, it is important to note the following:

1. Since the standard deviations of transport estimates are at least an order of magnitude greater than the means, it is unlikely that the values are representative of the long-term (climatologic) mean. The "means" calculated here are highly influenced by a few events that may or may not be characteristic of the area. The single storm event which exhibited 71 cm/s orbital wave velocities on December 14, 1988, for example, resulted in maximum westward transport of 6.8 cm^2/s at mooring 1C. This single event, averaged over the entire deployment period, would produce a "mean" transport larger than the mean at any other site by an order of magnitude. Only after careful use of the historical wind data and both wind-current and wind-wave relationships (beyond the scope of this report) will it be possible to build a dynamical model accurate enough to define the long-term sediment transport.

2. These vertically integrated transport estimates are not the same as the net sediment transport. Estimates reported in Table 4 simply represent a "flux" of sediment past specific points. Calculating the spatial gradients of these transport estimates, however, will provide estimates of net deposition/erosion rates. To accomplish this task, it will be necessary to apply numerical box modeling techniques to a dense grid of stations that accurately represents changes in bathymetric gradients and oceanographic conditions. Spatial derivatives (due the changes of surficial sediments, orbital wave velocities, and currents) are needed to accurately estimate sediment transport throughout the region. A preliminary investigation of deposition/erosion and further discussion of net sediment transport are presented in a subsequent section.

3. Finally, how does sediment grain size affect the model results? The sediment transport estimates have not included a depth of erosion limit. *Lyne et al.* [1990] demonstrated the importance of this adjustment to making predicted resuspension agree with that measure by transmission observations. As the fine grain deposits are depleted during a particular event, there is inevitably a change in the magnitude of resuspension as the composition of the bed load is modified to include mostly larger sand grains. (Estimates of bed load transport are not included in the numbers reported here.) It is therefore possible that the smaller events depicted in the stick plot in Figure 8 may be as "significant" as the larger events in terms of reworking the available fine-grained material.

In other words, there is a temporal variability in the composition of surficial fines that is not included in the model parameterization. As *Packer et al.* [1994] have observed during the period of this study, the dominant grain size at a particular site may change by a few orders of magnitude over the period of the model run (see Table 2). The few observations by *Hathaway* [1971] therefore may be a biased representation of the mean grain size distribution. To investigate the influence of grain size input, a sensitivity test was conducted for the record at mooring 3B (November 1988-June 1989). The model was run several times with grain size input varying from 100% sand (.1 cm) to 100% silt (.006 cm) in increments of phi size (0-4). As the diameter of the grain is reduced by half, the resultant sediment transport increased by approximately an order of magnitude. The rate of increase is slightly less for the smaller grain size as stratification begins to take effect.

However, the results reported in Table 4 and in Figure 8 indicate the frequency, the direction, and the order of magnitude of sediment transport to be expected at the mooring locations themselves. Several other sensitivity tests were conducted. Other alterations in the model input variables tended to affect the final results by less than an order of magnitude. These alterations included (1) not applying the 9-hour phase lag for Ambrose Light Tower versus Nantucket waves, (2) applying a correction factor for the cohesiveness of the sediment, and (3) using nonfiltered current velocities. Since the space and time variability of the estimates spans several orders of magnitude, it appears that the model is sufficiently robust for purposes of this study.

The seasonality of sediment transport reported in Table 4 is in fact what one might expect from the wind-current relations described above. Estimates from moorings deployed during the winter of 1988-1989 (1C, 3B, and 9B) are

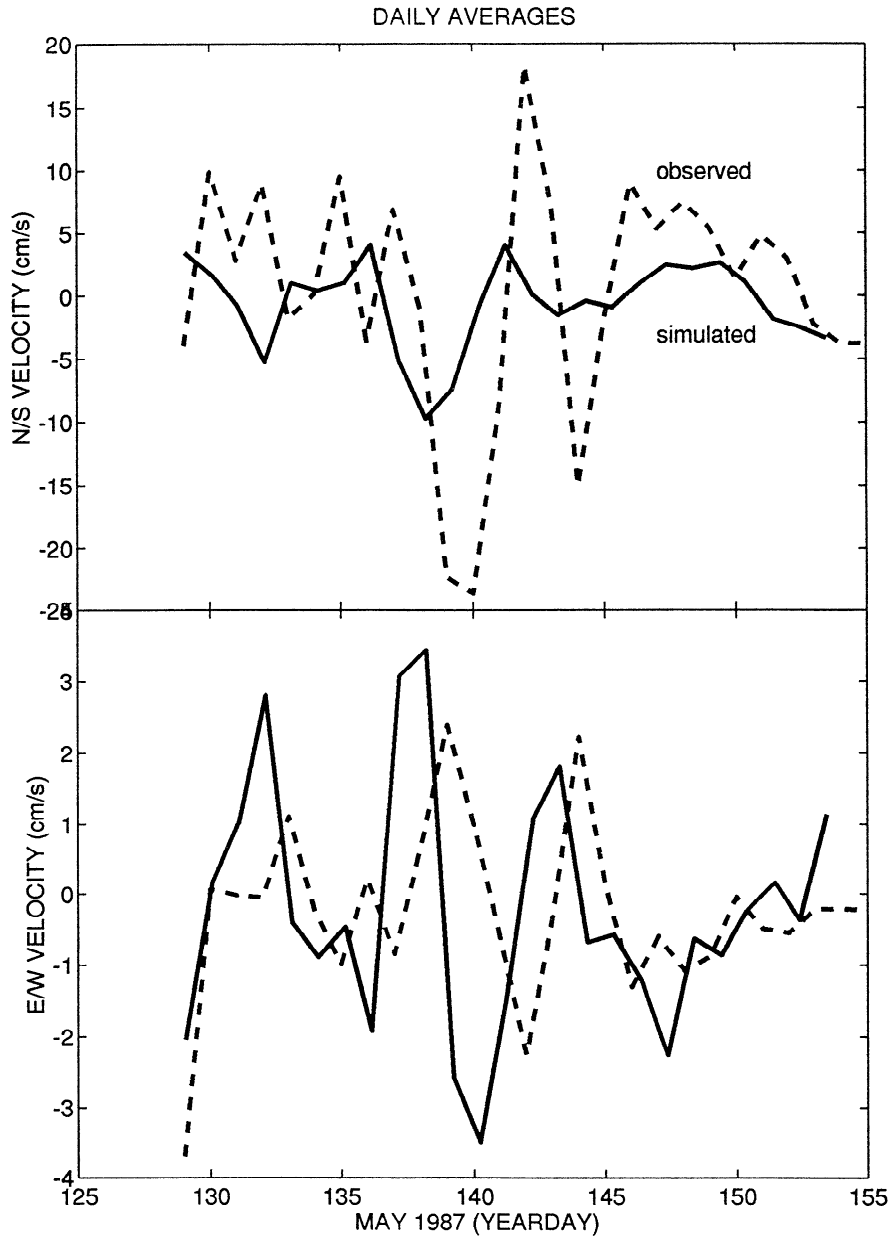

Figure 6. Simulated (solid) and observed (dashed) near-bottom current for May 9 - June 3, 1987. Top panel is the north/south (along-valley) flow, (-25 to 20 cm/s) and the bottom panel is the east/west flow (-4 to 4 cm/s). Low passed velocities are shown in both cases.

at least an order of magnitude larger than the estimates from summer deployments. (The only exception to this observation is the case of mooring 6 which, because of a single downwelling event in late May 1987, has a mean southerly transport of 0.000325 cm^2/s).

The conclusion that fall and winter storm events dominate the overall annual transport is in agreement with other recent findings on the northeast continental shelf [*Lyne et al.*, 1990]. Tracer studies conducted in this area by *Lavelle et al.* [1978], for example, found nearly 90% of the transport occurred within a single 2-day December storm over a 135-day period in the fall of 1973. A 2-year time series of sediment trap data from Boston Harbor [*Butman et al.*, 1992] indicates that there may actually be more resuspension during fall storms because of increased deposition during the relatively quiet summer months immediately proceeding this period.

Event Analysis

It is instructive to take a closer look at a few of the events that are so important to the long-term sediment transport, beginning with a wind event depicted on the top panel of Figure 11. When the west winds (blowing eastward off the New Jersey coast) apply stress that moves the surface waters to the right (southward), there is a compensating return flow at depth (dashed line in middle panel) that is directed up the Hudson Shelf Valley to the north with a lag time of approximately 18 hours. During the upvalley events on December 29 and January 4 and the downvalley event of January 7, the

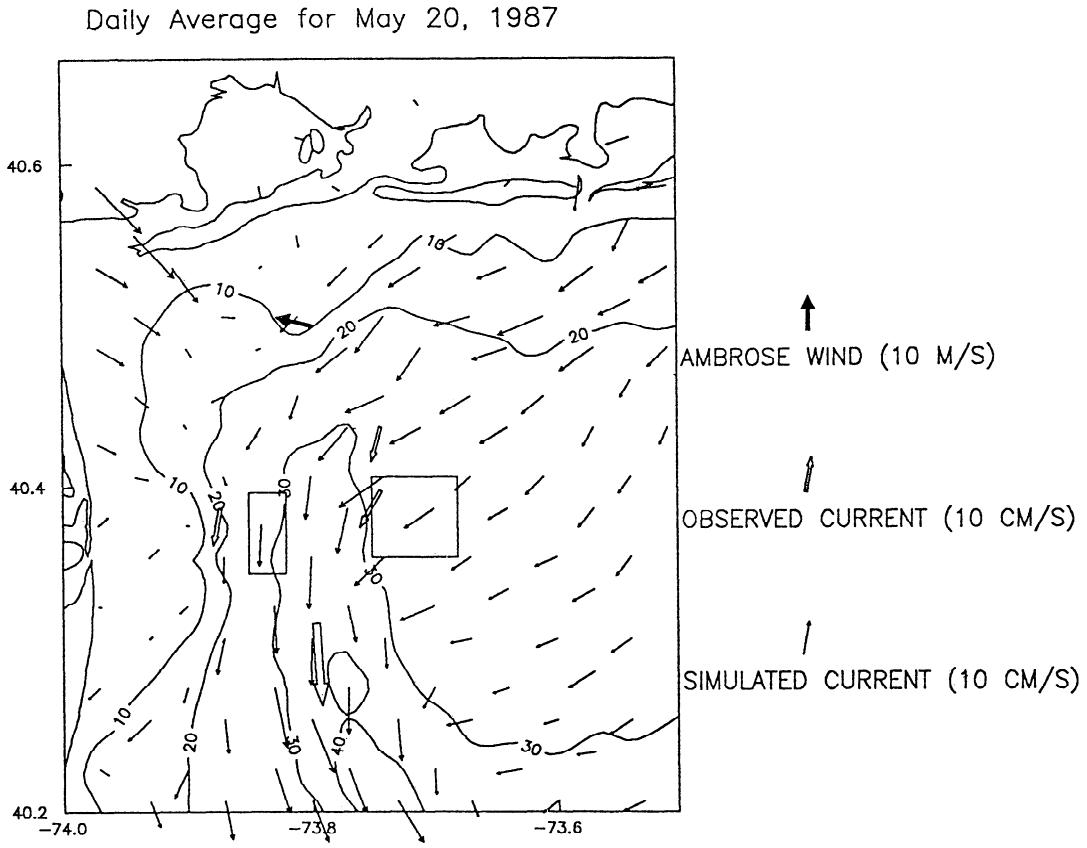

Figure 7. Vector map of simulated and observed current distribution averaged over May 20, 1987 (24 hr). Observed current is represented by the wide open arrows. Simulated current is shown at each grid point as a thin solid arrow. Wind speed at Ambrose Light Tower is shown by the wide solid arrow. The rectangle and square represent the dredge spoil and sewage sludge sites, respectively.

surface waves generated orbital velocities at the bottom on the order of 20 cm/s (solid line in middle panel). If, however, the surface wave energy had been lower or out of phase with the along-valley flow event, little or no transport would have occurred. The sediment transport events, shown in the bottom panel, have a typical duration of less than 24 hours.

Deposition/Erosion: Temporal Variability

Greater water depth offshore (see Figure 12) decreases wave-induced resuspension which, in most cases, tends to decrease the amount of sediment transport. Given the characteristics of an idealized box representing the area of the Christiaensen Basin, the model estimates episodes of both deposition and erosion. While deposition slightly exceeds erosion during this period of investigation, the difference is no greater than the storm-to-storm variability and is likely to be less than errors involved in the simplistic assumptions.

Probably the most simplistic assumption is that the sediment concentrations are in equilibrium with the calculated bottom stress. A realistic model needs to account for (1) the sediment resuspended elsewhere and advected into the box and (2) the sediment that remains in suspension after the storm-induced conditions relax. Both flux through the boundaries and poststorm redistribution of residual concentrations of fine-grained particles by subcritical flow is not included in this very primitive model.

Nevertheless, three storms were examined. On November 21, 1988, the model estimates an event (Figure 13, left panel) which was at first depositional and later erosional (net = +0.01 mm). During the first half of this storm the observed current was significantly less at mooring 3. Despite the larger orbital wave velocities at mooring 3, the sediment was deposited because the sediment transport leaving the basin was less than that entering. Later in the storm, however, the sediment was eroded because, while the current speeds at the two locations were similar in magnitude, the increased wave-induced resuspension at the shallower site tended to carry more sediment out of the basin than entered. The storm that occurred on January 21, 1989 (Figure 13, middle panel), was a depositional event (net = +0.021 mm) while that which occurred on April 14, 1989 (Figure 13, middle panel), was an erosional event (net = -0.0016 mm). The brief nature of these events suggest that the phase and magnitude of the tidal flow needs to be included in future model runs.

If the offshore decrease in orbital wave velocity was the only along-valley gradient in the input parameters, one would expect deposition and erosion during periods of downvalley and upvalley flow, respectively. Examination of these events, however, indicates that the alongvalley gradient in

Table 4. Estimates of Vertically Integrated Sediment Transport

Station	No. of points	EAST				NORTH				Seasons
		Mean	Standard	Minimum	Maximum	Mean	Standard	Minimum	Maximum	
1A	837	0.000000	0.000000	0.000000	0.000000	0.000000	0.000000	-0.000000	0.000000	Su
1B	1660	-0.000003	0.000045	-0.001633	0.000067	0.000002	0.000034	-0.000003	0.001165	Su
1C	5283	-0.001448	0.093110	-6.759000	0.008456	-0.000142	0.008543	-0.602000	0.023240	WSp
3A	711	0.000000	0.000000	0.000000	0.000001	0.000000	0.000000	0.000000	0.000006	Su
3B	4501	-0.000194	0.002481	-0.054550	0.001362	0.000187	0.003582	-0.038760	0.063280	WSp
4	2293	0.000000	0.000005	-0.000108	0.000060	-0.000007	0.000111	-0.003973	0.000000	Su
5	1384	-0.000004	0.000039	-0.001033	0.000000	-0.000010	0.000103	-0.002605	0.000001	Su
6	2568	0.000019	0.000229	-0.000088	0.005868	-0.000325	0.003781	-0.089830	0.000004	Su
9b	7427	-0.000011	0.002537	-0.033610	0.072400	0.001506	0.022900	-0.088630	0.565000	WSpSuF

Transport units are in centimeters squared per second. Seasons are Su, summer; W, winter; Sp, Spring; and F, fall.

Table 5. East/West Wind Stress and North/South Current Relationships for the 2-10 Day Band

Station	Coherence		Transfer Function				Record Length
	Estimate	95% Confidence Limit	Gain	Confidence Interval	Phase deg.	Confidence Interval	days
1A	0.77	0.44	4.3	1.7	29	27	27
1B	0.51	0.38	3.1	2.2	65	25	103
1C	0.71	0.17	5.0	0.9	50	20	220
2	0.78	0.34	7.4	2.2	37	14	49
3A	0.48	0.24	6.5	2.9	78	28	114
3B	0.59	0.24	6.5	1.7	85	26	187
4	0.73	0.26	5.2	1.3	9	16	88
5	0.70	0.34	9.2	3.4	0	14	55
6	0.66	0.24	13.0	3.8	3	15	88
9B	0.63	0.13	11.6	1.9	71	23	337

Gain units are cm/s per dynes/cm^2.

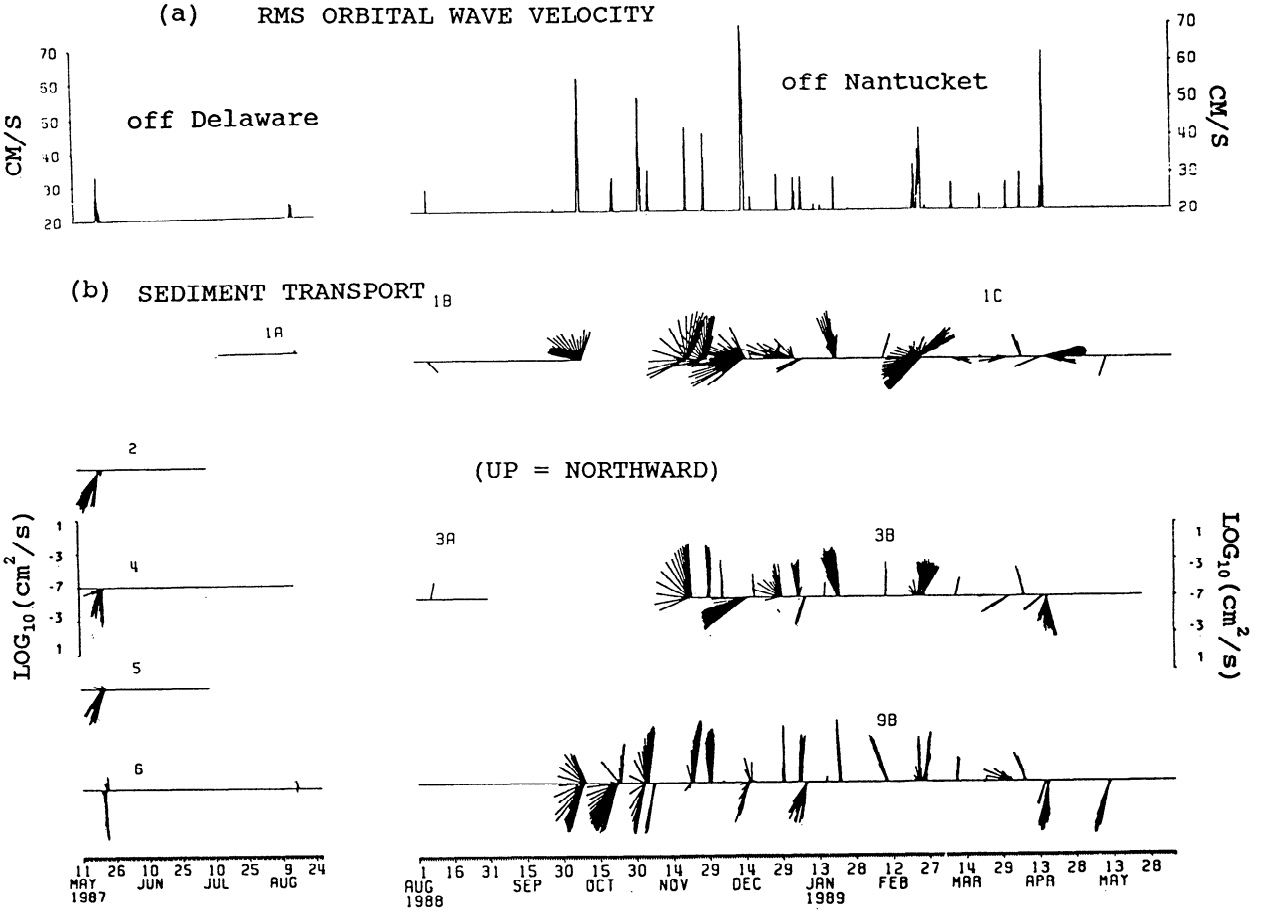

Figure 8. (top) Rms orbital wave velocities (>20 cm/s) and (bottom) sediment transport estimates ($\log_{10}(cm^2/s)$).

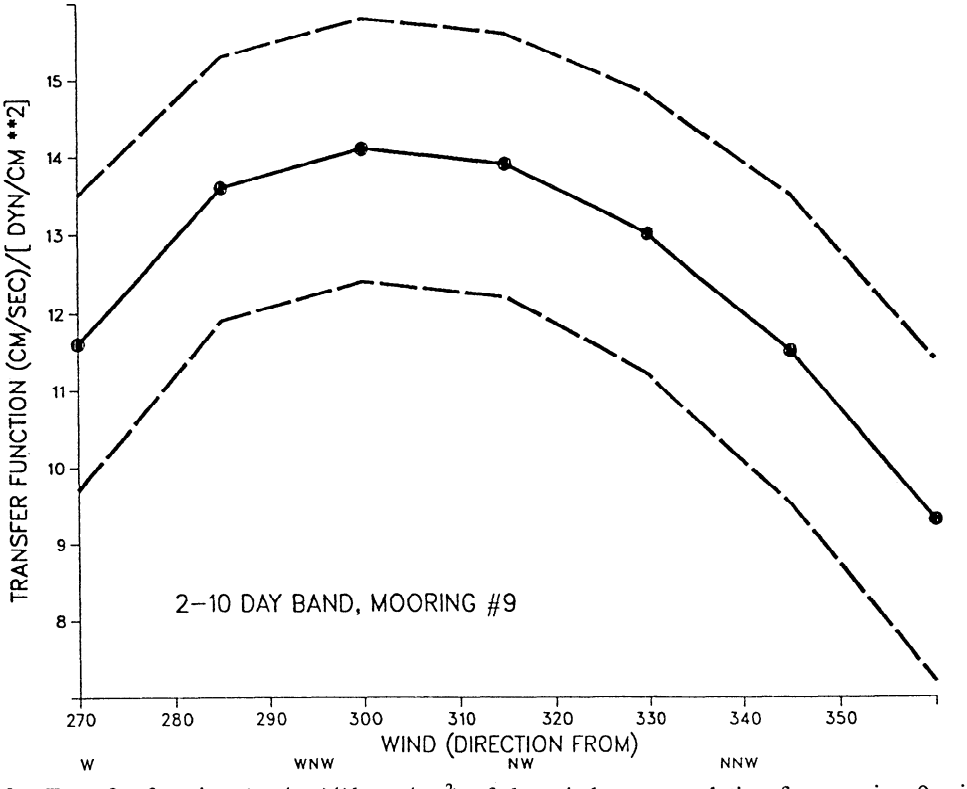

Figure 9. Transfer function (cm/sec)/(dynes/cm^2) of the wind-current relation for mooring 9 with one point per 15° of the compass (solid line). Dashed lines represent the 95% confidence limits. Peak efficiency occurs for wind from the WNW.

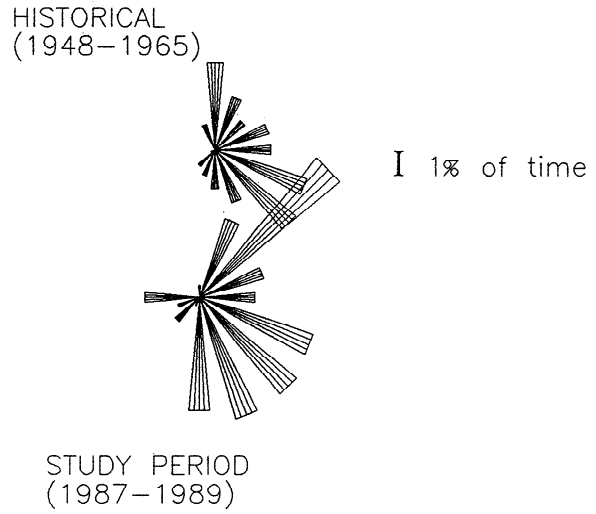

bottom flow may be important as well. Hence in order to resolve the spatial variability of the model input parameters, it will be necessary to implement the three-dimensional circulation models (wind-driven, time-dependent) currently under development at various agencies [*You et al.*, 1991; *Blumberg and Galperin*, 1990; and Army Corps Waterways Experiment Station, personal communications, 1993] and discussed briefly in the following section.

Figure 10. Directional distribution of strong winds during the historical (1948-1965, NYC/JFK airport) and study period (1987-1989, Ambrose Light Tower). "Strong" winds for NYC/JFK are those greater than 11 knots. "Strong" winds for Ambrose Light Tower are those greater than 12.2 knots. A gain factor of 1.11 came from the difference in the long-term mean wind speeds of the two data sets.

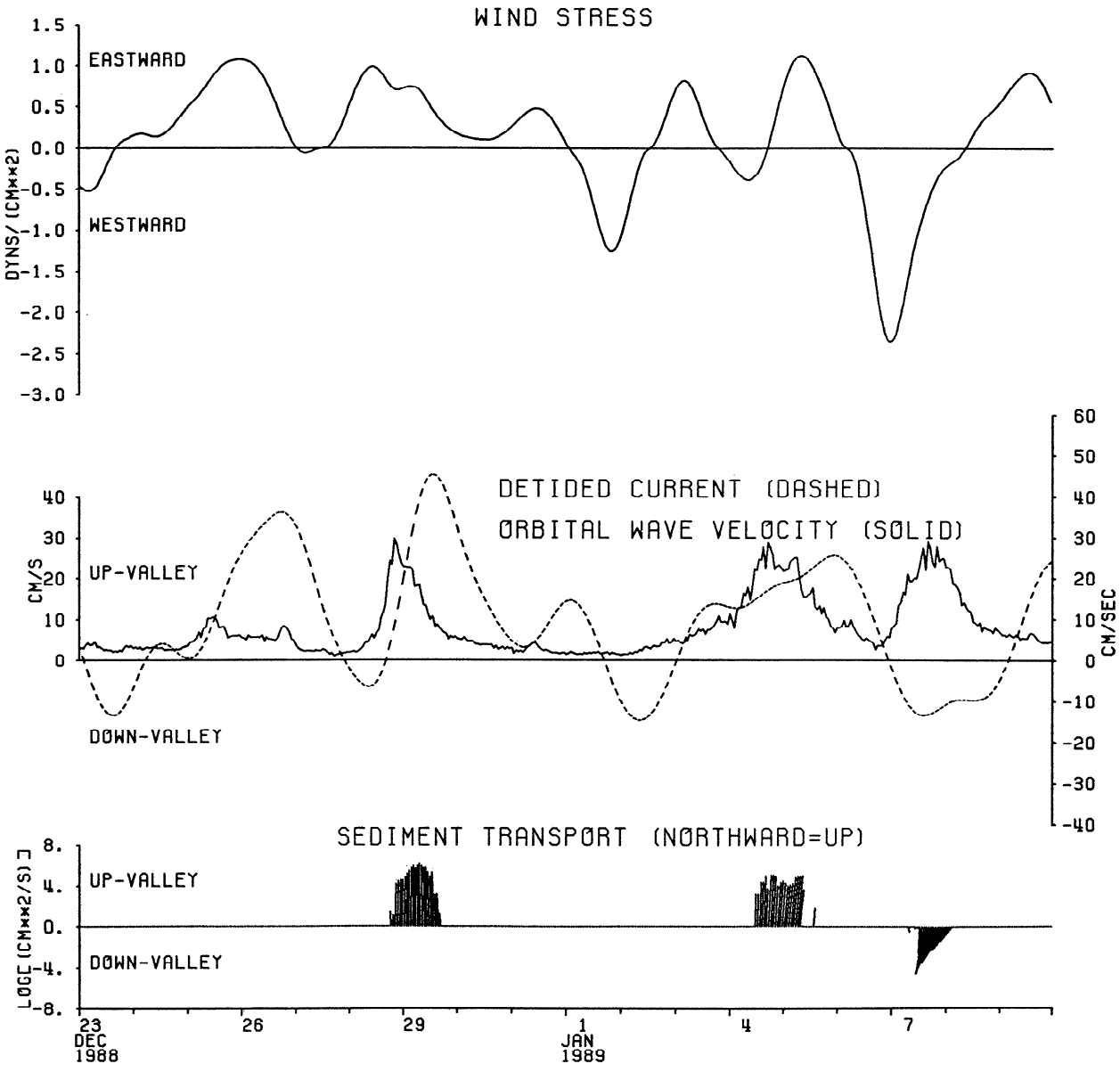

Figure 11. Example of three sediment transport events including the wind stress, both the rms orbital wave velocity (solid line) and the subtidal flow (dashed line), and estimate of log transformed resuspended transport in cm^2/s.

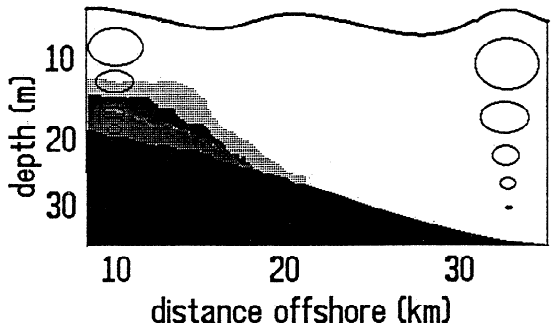

Figure 12. Schematic of along-valley differences in wave-induced sediment resuspension. The solid black area represents the bathymetry sloping in-shore to off-shore. The stippled area represents resuspended sediment. It is especially heavy in the shallower sites. Spatial gradients in wave-induced resuspension and other model input parameters are needed to estimate **net** sediment transport (see text). The ellipses represent the rough form of orbital motion due to waves.

Deposition/Erosion: Spatial Variability

Output from circulation model of *You et al.* [1991] is used for a particular storm period of May 17-24, 1987 to examine the potential redistribution of sediment under a set of constant surface wave conditions. While the quantity of deposition/erosion varied for the different cases of wave height and period (2 m/20 s, 2 m/10 s, 1 m/10 s, .8 m/8 s), the spatial distribution remained very similar for all cases. With the assumption that wave height and period is constant in space, the orbital wave velocity and excursion amplitude varies according to water column depth (Figure 14a). It appears that for the late May 1987 storm the areas of deposition and erosion corresponded to areas of deep and shallow water, respectively Figure 14b), but there are factors other than the variable influence of the surface waves, such as spatial variability in current, that contribute to the redistribution of sediment. In the future, when the wind-wave hindcasting models are developed for the inner New York Bight at 1-2 km resolution for this study period, it will possible to portray a more accurate representation of the sediment dynamics.

There are sediment data available that support the hypothesis of depositional regions associated with the deeper depressions (Hudson Shelf Valley, Christiaensen Basin). Broadscale surveys of the surficial sediment characteristics, when averaged over several cruises, depict a fine siltlike sediment in the deeper regions and a coarse sandlike sediment in the shallows (Figure 14c and 14d). Earlier well-documented MESA studies [*Stubblefield, et al.*, 1977] and the preliminary results presented here indicate a very patchy distribution of surficial fines such that a higher resolution sampling with side-scan sonar is needed to accurately map the area. Hence, in the future, if this sediment transport model (or those similar to it) becomes fully operational, it

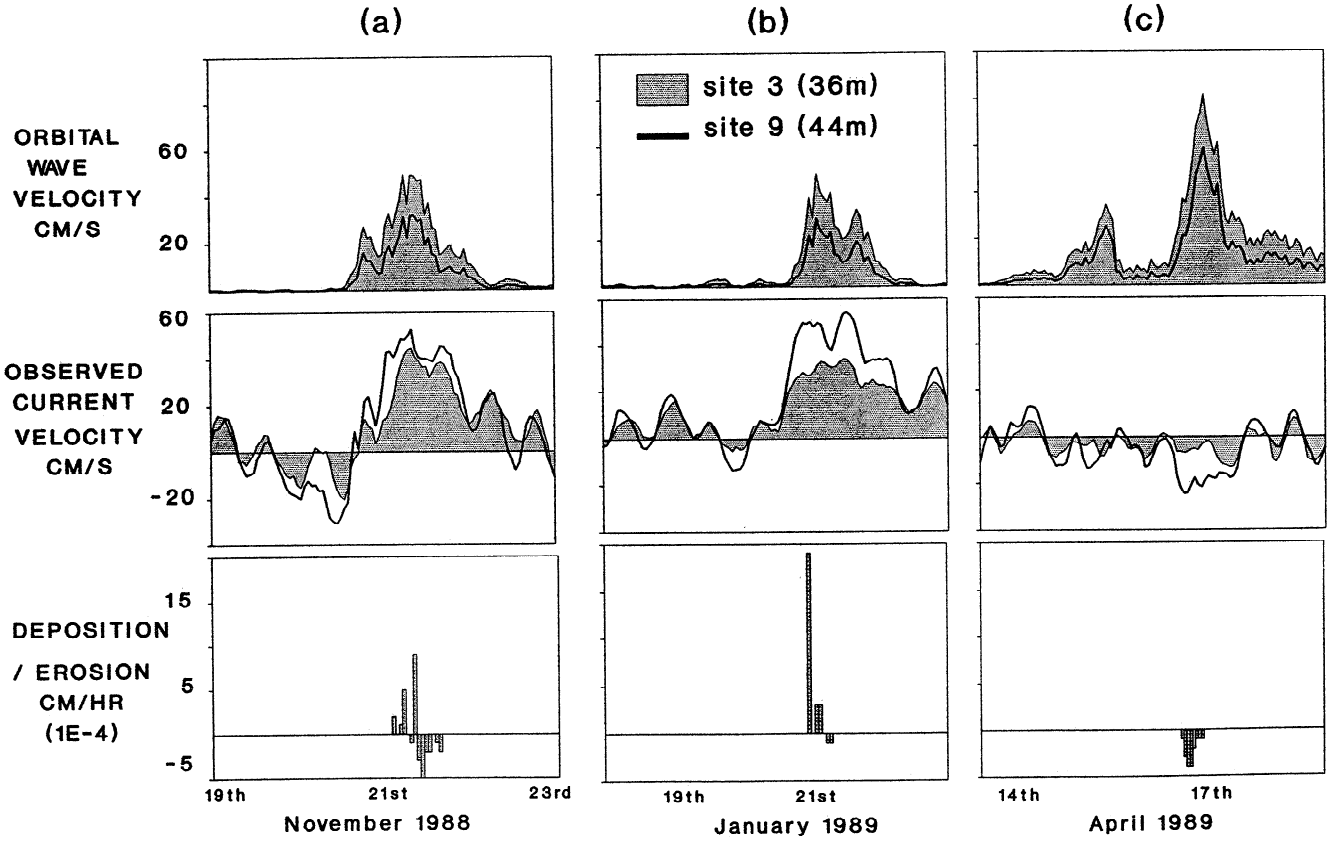

Figure 13. The left, middle, and right panels are examples of mixed, depositional, and erosional events, respectively, that may occur because of spatial gradients in orbital wave velocity (top panels) and residual currents (middle panels). The simple model, presented for discussion purposes only, uses the differences between mooring 3 (shaded) and 9 (solid line) to estimate deposition/erosion rates (bottom panels).

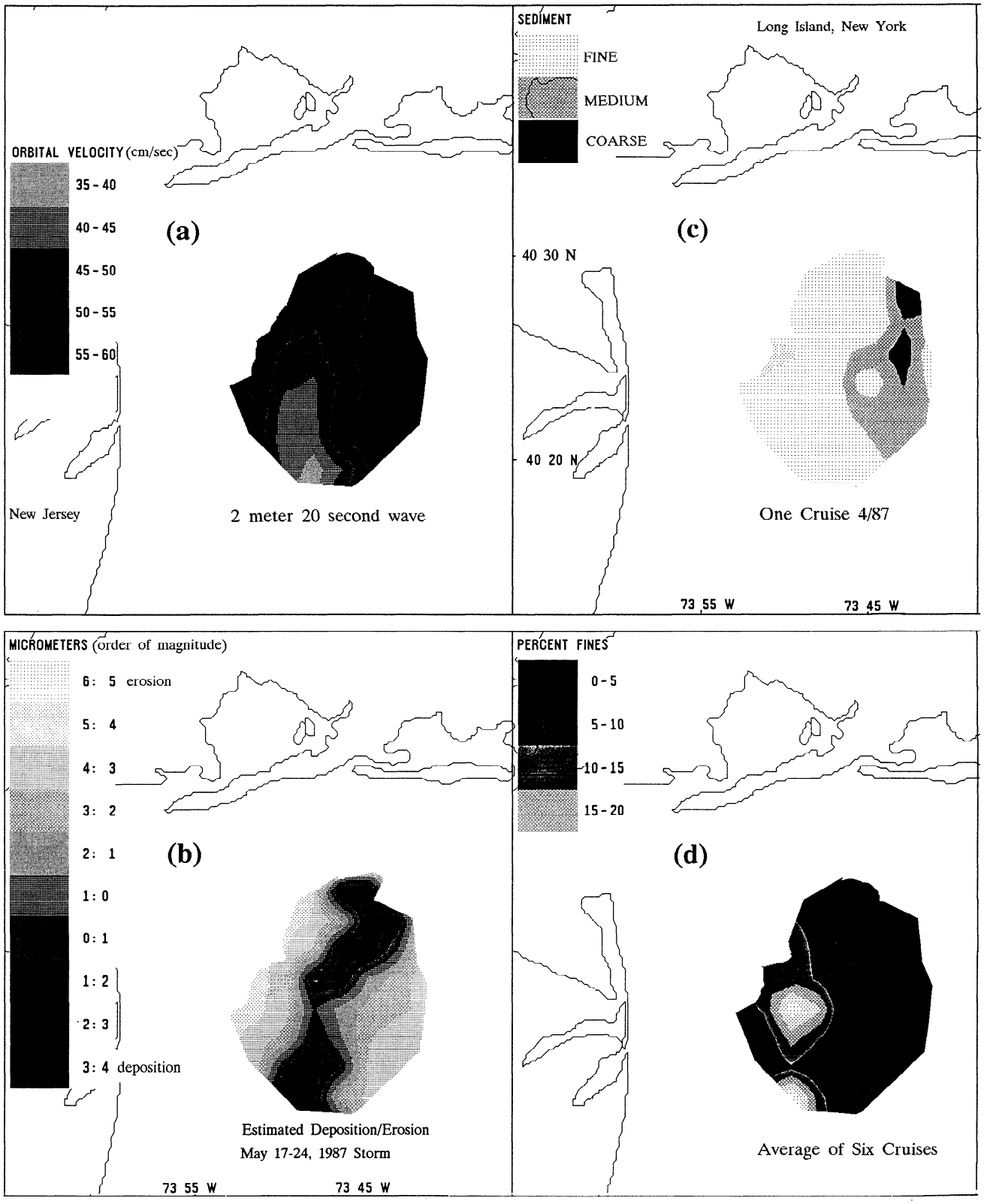

Figure 14. Spatial distribution of orbital wave velocity given a 2 m/20 second wave (a), estimated deposition/erosion given those orbital wave velocities together with circulation model output for May 17-24, 1987 (b), sediment type observed in April 1987 (c), and percent fines averaged over six cruises (d).

will be necessary to have fine scale sediment samples to validate the results. The addition of sediment core samples may also help to determine the long-term history of deposition/erosion.

Summary

The subtidal flow field in the vicinity of the 12-mile dumpsite is coherent between sites, especially for the along-valley flow (.82-.94) and less so for the cross-valley flow (.54-.62). Phases between sites are all less than a half day for the 2-10 day storm band.

West-northwest winds, dominant during the winter months, are most efficient in forcing northward flow both within the Hudson Shelf Valley (40-60 m) and at sites on the shallower flanks (20-40 m), often in excess of 25 cm/s for several days duration. During the remainder of the year, the flow magnitude is approximately half as large, and flow direction is more variable.

A continental shelf bottom boundary layer model was applied using the observations of bottom currents, bottom wave characteristics, and sediment grain size data in order to obtain order-of-magnitude estimates of resuspended sediment transport at all sites. The most significant conclusions in terms of sediment transport are (1) very few events contribute to the annual transport at any one site, (2) the resuspended transport estimates are dependent on the simultaneous occurrence of waveinduced resuspension and wind-induced flow, and (3) the frequency and magnitude of the transport increases in the winter and is usually directed upvalley.

Only with careful attention to the direction of bottom flow events, the statistical probability of flow events occurring simultaneously with wave-induced resuspension events, and the spatial gradients of these events throughout the inner New York Bight, can one undertake the very difficult task of estimating the net transport of sediment in this very complex environment. Recent three-dimensional circulation models show promise as a very valuable tool that, if coupled with the surface wind-wave and the bottom boundary layer models, will undoubtedly contribute to our understanding of sediment dynamics in the New York Bight.

Acknowledgements. We thank all those involved in the initial planning and operation of the 12-mile dumpsite study, Bill Phoel for leading the sediment lab at Sandy Hook, and Ron Schlitz for coordinating the physical oceanographic moorings. We thank all those who provided software: Scott Glenn for the bottom boundary layer model, Jim Churchill for bottom wave velocity model, and Rich Signell for various subroutines. The support of the National Center for Supercomputing Applications, Illinois, where the three-dimensional model calculation was performed, is acknowledged. We thank all the reviewers of this manuscript, particularly Jay O'Reilly, Mert Ingham, and David Mountain.

References

Blumberg, A.F., and B. Galperin, On the summer circulation in the New York Bight and contiguous waters, in Residual Currents and Long-term Transport, *Coastal Estuarine Stud., vol. 38*, edited by R.T. Cheng, AGU, Washington, D.C., 1990.

Butman, B., M.H. Bothner, J.C. Hathaway, H.L. Jenter, H.J. Knebel, F.T. Manheim, and R.P. Signell, Contaminant transport and accumulation in Massachusetts Bay and Boston Harbor: Summary of U.S. Geological Survey results, *U.S. Geol. Surv. Open File Rep., 92-202*, 1992.

Clarke, T.L., B. Lesht, R.A. Young, D.J.P. Swift, and G.L. Freeland, Sediment resuspension by surface wave action: An examination of possible mechanisms, *Mar. Geol., 49*, 42-59, 1982.

Environmental Processes Division, Plan for study: Response of the habitat and biota of the Inner New York Bight to abatement of sewage sludge dumping, Northeast Fisheries Sci. Cent., Woods Hole, Ma., 1987.

Flagg, C.F., The kinematics and dynamics of the New England Continental Shelf and shelf/slope front, PhD. thesis, 208 p., Woods Hole Oceanographic Insti.-Massachusetts Insti. of Tech., WHOI-77-67, 1977.

Gadd, P.E., J.W. Lavelle, and J.P. Swift, Estimates of sand transport on the New York Shelf using near-bottom current meter observations, *J. Sediment Petrol.*, 48(1), 239-252, 1978.

Glenn, S.M., and W.D. Grant, A continental shelf bottom boundary layer model, *Users manual, vol. III*, technical report, 186 pp., Am. Gas Assoc., Arlington, Va., 1983.

Glenn, S.M., and W.D. Grant, A Suspended Sediment Stratification Correction for Combined Wave and Current Flows, *J. Geophys Res, 92(C8)*, 8244-8264, 1987.

Goud, M.R., Prediction of continental shelf sediment transport using a theoretical model of the wave-current boundary layer, Ph.D. thesis, Woods Hole Oceanogr. Inst., Woods Hole, Mass., 1987.

Grant, W.G., and O.S. Madsen, 1979, Combined wave and current interaction with a rough bottom, *J. Geophys. Res., 84*, 1797-1808, 1979.

Han, G.C., D.V. Hansen, and J.A. Galt, Steady-state diagnostic model of the New York Bight, *J. Phys. Oceanogr., 10*, 1998-2020, 1980.

Hathaway, J.C., Data file continental margin program Atlantic Coast of the United States, vol. 2, Sample collection and analytical data, *Tech. Rep. WHOI-71-15*, 496 pp., Woods Hole Oceanogr. Inst., Woods Hole, Mass., 1971.

Large, W.G. and S. Pond, Open ocean momentum flux measurements in moderate to strong winds, *J. Phys. Oceanogr., 11*, 324-336, 1981.

Lavelle, J.W., J.P. Swift, P.E. Gadd, W.L. Stubblefield, F.N. Case, H.R. Brashear, and K.W. Haff, Fair weather and storm sand transport on the Long Island, New York, inner shelf, *Sedimentology, 25*, 823-842, 1978.

Lyne, V.D., B. Butman, and W.D. Grant, Sediment movement along the U.S. east coast continental shelf- II. Modelling suspended sediment concentration and transport rate during storms, *Cont. Shlf. Res., 10(5)*, 429-460, 1990.

Mayer, D.A., G.C. Han, and D.V. Hansen, Circulation in the Hudson Shelf Valley: MESA physical oceanographic studies in the New York Bight, 1, *J. Geophys. Res., 87* (C12):9563-9578, 1982.

Nelson, T.A., P. Gadd, and T. Clarke, Wind-induced current flow in the upper Hudson Shelf Valley, J. Geophys. Res., 83:6073-6082, 1978.

O'Reilly, J.E., I.J. Katz, and A.F.J. Draxler, Changes in the Abundance and distribution of Clostridium perfringes, a microbial indicator, related to cessation of sewage sludge dumping in the New York Bight, in Sewage Sludge Dumping in the Inner New York Bight: Response of the Habitat and Biota to the Closure of the 12-Mile Site, edited by A.L. Studholme, J.E. O'Reilly, and M.C. Ingham, NOAA Tech. Mem. NMFS-F/NEC, in press, 1994.

Packer, D., T. Finneran, L. Arlen, R. Koch, S. Fromm, J. Finn, A. Draxler, Fundamental and mass properties of

surficial sediments in the Inner New York Bight and responses to the abatement of sewage sludge dumping, in Sewage Sludge Dumping in the Inner New York Bight: Response of the Habitat and Biota to the Closure of the 12-Mile Site, edited by A.L. Studholme, J.E. O'Reilly, and M.C. Ingham, NOAA Tech. Mem. NMFS-F/NEC, in press, 1994.

Stubblefield, W.L., R.W. Permenter, and D.J.P. Swift, Time and space variation in the surficial sediments of the New York Bight apex, *Estuarine Coastal Mar. Sci., 5*, 597-607, 1977.

Studholme, A.L., M.C. Ingham, and A. Pacheco, Response of the habitat and biota of the Inner New York Bight to abatement of sewage sludge dumping: Third annual progress report, *NOAA Tech. Rep. NMFS-F/NEC, 82*, 57p., 1991.

Vincent, C.E., R.A. Young, and J.P. Swift, Bed load transport under waves and currents, Mar. Geol., 39, 71-80, 1981.

You, K.W., A 3-D model simulation of circulation and mixing in the New York Bight, Ph.D. thesis, 133 p., Stevens Inst. of Technol., Hoboken, N.J., 1992.

You, K.W., L.Y. Oey, H.T. Jo, P. Chen, J.P. Manning, R. Patchen, and J. Herring, A 3-D simulation of buoyancy and wind-induced circulation and mixing in the New York Bight, paper presented at Estuarine and Coastal Modeling, 2nd International ASCE Conference, Tampa, Fl., Nov. 13-15, 1991.

Zdanowicz, V.S., S. Leftwich, and T.W. Finneran, Reductions in sediment metal concentration in the New York Bight Apex with the cessation of sewage sludge dumping, in Sewage Sludge Dumping in the Inner New York Bight: Response of the Habitat and Biota to the Closure of the 12-Mile Site, edited by A.L. Studholme, J.E. O'Reilly, and M.C. Ingham, NOAA Tech. Mem. NMFS-F/NEC, in press, 1994.

T. W. Finneran, S. From, D. Packer, J. Vitaliano, National Marine Fisheries Service, National Oceanic and Atmospheric Administration, James J. Howard Laboratory, Highlands, NJ 07732.

J. P. Manning, National Marine Fisheries Service, National Oceanic and Atmospheric Administration, Woods Hole, MA 02543.

L. Y. Oey, Atmospheric and Ocean Sciences Program, Princeton University, Princeton, NJ 08542.

K. W. You, Department of Civil, Environmental, and Ocean Engineering, Stevens Institute of Technology, Hoboken, NJ 07030.

(Received October 20, 1992; revised August 2, 1993; accepted October 15, 1993.)